Monetizing Shale Gas to Polymers under Mixed Uncertainty: Stochastic modeling and likelihood analysis

Chang He*, Ming Pan, Bingjian Zhang, Qinglin Chen

School of Chemical Engineering and Technology, Guangdong Engineering Center for Petrochemical Energy Conservation, Sun Yat-sen University, Guangzhou, 510275, China.

Fengqi You

Robert Frederick Smith School of Chemical and Biomolecular Engineering, Cornell University, Ithaca, New York 14853, USA

Jingzheng Ren

Department of Industrial and Systems Engineering, The Hong Kong Polytechnic University, Hong Kong Special Administrative Region, China

Submitted to *AIChE Journal*

*Corresponding authors: Chang He, E-mail addresses: hechang6@mail.sysu.edu.cn.

Abstract

This paper presents a novel framework based on stochastic modeling methods and likelihood analysis to address large-scale monetization processes of converting shale gas to polymers under the mixed uncertainties of feedstock compositions, estimated ultimate recovery, and economic parameters. A new stochastic data processing strategy is developed to quantify the feedstock variability through generating the appropriate number of scenarios. This strategy includes the Kriging-based surrogate model, sample average approximation and the integrated decline-stimulate analysis curve. The feedstock variability is then propagated through performing a detailed techno-economic modeling method on distributed-centralized conversion network systems. Uncertain economic parameters are incorporated into the stochastic model to estimate the maximum likelihood of performance objectives. The proposed strategy and models are illustrated in four case studies with different plant locations and pathway designs. The results highlight the benefits of the hybrid pathway as it is more amenable to reducing the economic risk of the projects.

Keywords: stochastic modeling, likelihood analysis, shale gas, mixed uncertainty, techno-economic modeling.

Introduction

The recent surge in global natural gas supply accompanying shale gas production has notably underpinned the petrochemical industries with sufficient feedstocks like methane and natural gas liquids (NGLs, C_2H_6, C_3H_8, and C_{4+}).[1] However, it is well-known that the shale gas producers in North America are in a pessimistic economic climate recently due to the collapse of oil prices. The Henry Hub price[1] of natural gas has dropped significantly from $6.00/mmbtu in February 2014 to $2.28/mmbtu in January 2016, causing shale gas projects to suffer deficits under current drilling costs (>$3.00/mmbtu). Increased attention has been paid to the development of promising routes to cost-effectively transform shale gas into more valuable products for end-use customers. These products include, but are not limited to, alcohol, F-T oil, polymers, aromatics, pipeline gas (PG), and electricity.[2] Among them, polymers and their derivatives have been extensively used in an expanding range of products from paper clips to spaceships, due to their versatile nature and ease of transportation and storage. Since 1980, global polymers production has increased by an average annual growth rate of around 5%, resulting in the total production up to 311 million metric tons (Mt) in 2014.[3] This strong demand stimulates industries to utilize shale gas as the feedstock for complementing the current petroleum-based polymers production.

The important issues addressed in shale gas monetizing processes are process design and the synthesis of end-use products.[2] Steam cracking of NGLs has been proposed as a technically mature approach to monetizing shale gas to lighter olefins in industry. It is noted that olefins presenting in the atmosphere in vapor form require a cryogenic environment for transporting and storage, leading to very high transportation costs. Alternatively, producing polymers from NGLs through steam cracking and olefin polymerization in series would mitigate the above issues and improve the economics of shale gas projects under the current low price of natural gas. The shale gas boom has also increased the interest in C_1 chemistry by converting it to

chemicals via various technologies. This has been a controversial issue in shale gas projects for a long time. However, a direct and one-step route of methane conversion, namely the oxidative coupling of methane (OCM) reaction,[4] can produce products involving similar components obtained from the NGLs cracking gas after being sweetened. This technology leads to great opportunities for process integration, gas co-processing, and equipment sharing, which potentially reduces the normalized energy usage and capital cost.[2,5] Thus in the monetization of shale gas (like NGLs), methane becomes an attractive feedstock in relation to carbon efficiency and economic competitiveness, but there are only limited literature on process design and integration that explore such potential opportunities.

Increasing scientific evidence is showing that the shale gas monetizing process is inevitably subject to mixed and multi-dimensional uncertainties from gas acquisition to end-use production, which significantly affects the profitability and environmental impacts of the whole project. First, raw shale gas acquisition (the initial step of shale gas projects) is most influenced by the endogenous uncertainties of gas compositions.[2,6-9] In fact, most of the shale gas regions (even different wells in the same region) produce raw shale gases with high compositional variabilities due to the differences in geological, geochemical, and petrophysical characteristics in these regions and wells. Meanwhile, the variability associated with shale gas acquisition refers to the estimated ultimate recovery (EUR), which is affected by the special decline in production rate and well-refracturing operation.[10-12] In addition, exogenous uncertainties normally occur throughout the entire project caused by market variabilities such as product prices, drilling costs, utility prices, and significantly increases the complexity of uncertainty in practice.[13] The resulting mixed uncertainties must be explicitly figured out at the design and development stage.

In light of the aforementioned issues, this work seeks to develop a new systematic framework that is capable of investigating large-scale processes of monetizing shale gas to

polymers under mixed uncertainties, including feedstock compositions, EUR, and economic parameters. To capture the feedstock variabilities, for the first step it proposes a new data processing strategy to generate appropriate scenarios from real-world data related to shale gas compositions and EUR. This strategy integrates three rigorous statistical methods, including the sample average approximation (SAA), the Kriging-based surrogate model (KSM), and the integrated decline-stimulate analysis curve (DSAC). Next, this work employs the detailed process design and techno-economic modeling, by which the raw shale gas in each scenario is processed in multi-site distributed processing facilities, and then either NGLs, or the mixture of NGLs and methane, can be pipelined to a centralized plant for polymer production. These generated scenarios are considered together with a set of uncertain economic parameters to identify their probabilistic distributions and techno-economic-environmental objectives based on likelihood analysis. Finally, the applicability of the proposed framework is illustrated through four case studies under different plant locations and monetization pathways.

The major novel contributions of this work are given as follows:

- This paper represents the first attempt to simultaneously address the uncertainties of EUR and feedstock compositions using a novel stochastic data processing strategy.
- New process design and techno-economic modeling of a hybrid pathway featuring the combination of converting C_1 and NGLs to polymers are developed.
- Uncertain economic parameters are fluidly incorporated into the stochastic model, and can be used to estimate the max-likelihood of process performances.
- Four practical case studies based on the real-world field data from the Appalachian and Golf Coast regions are provided.

The rest of this paper is organized as follows. After literature review, the overall monetization framework and conversion pathways are briefly introduced. Then, a three-step approach, including the quantification of feedstock variability, process design and techno-

economic modeling, and likelihood estimation is described in detail. Finally, four case studies are presented to demonstrate the applicability of the proposed methodology.

Literature Review

General information about process design, modeling, integration, and optimization of shale gas monetization processes can be found in several reviews.[2,14-16] These monetization processes can be classified into three categories, namely the C_1 pathway, NGLs pathway, and hybrid pathway. The current industrial practice of the C_1 pathway mainly involves the methane reforming technology, which generates syngas that can be further used as an intermediate to produce commodities. For example, El-Halwagi and co-workers[17] developed a syngas-based process for the production of methanol from shale gas. Later, by considering four reforming options and analyzing their sustainability performances, they found that the partial oxidation and auto-thermal reforming could have better economic performance, while the combined reforming outperformed other alternatives with the lowest carbon footprints.[18] Floudas and co-workers developed a number of process synthesis superstructures toward the production of aromatics,[19-21] light olefins,[22] and liquid fuels[23] from natural gas/shale gas via the syngas-based processes using methanol as intermediate. However, these syngas-based routes have been known for having large carbon footprints and low carbon efficiencies.[5,24] There is a growing interest in the C_1 direct conversion pathway using OCM reaction since it is potentially more economical and environmentally friendly,[4] i.e., Siluria Technologies[25] had developed industry-scale methane to chemical/fuel processes by discovering a bio-template and nanowire OCM catalysts. Salkuyeh and Adams[26] introduced a new poly-generation process to co-produce ethylene and electricity from shale gas with zero CO_2 emissions via OCM reaction. However, OCM pathway has a low conversion rate and high separation cost that lead to a number of commercialization barriers.

The NGLs pathway based on thermal pyrolysis of C_2-C_3 hydrocarbons is a major industrial approach for yielding the lighter olefins that mainly include ethylene and propylene. For example, U.S. petrochemical industries have announced that the cracking capacities are expected to be 14 Mt by 2020, and most of them employ reliable steam cracking technology. Recently, there are several studies on comparative techno-economic and environmental analysis for manufacturing olefins from shale gas via the same technology.[27,28] To achieve better project economics, He and You[29] proposed a co-processing strategy for integrating shale gas processing with ethylene production, and the co-processing of shale gas and ethane cracking gas. They also developed a mega-scale shale gas conversion network with an explicit consideration of process design and systems integration to investigate the water-energy-carbon nexus.[30] In addition, researchers have designed various novel hybrid pathways to improve the energy-economic-environmental performances of shale gas projects. There are two sub-groups of hybrid pathway designs, namely external integration, where the raw shale gas can co-feed with other types of resource, i.e. agricultural/forest residues,[31] bioethanol,[5] switchgrass,[32] pipeline gas,[33] etc. and internal integration, where the methane and NGLs included in raw shale gas have the potential to be integrated within the processing and production systems.[26,29,34]

As mentioned early, uncertainty is an inherent characteristic in a shale gas monetizing process, which leads to significant challenges in handling variability and/or stochasticity in parameter values. Typically, uncertainty can be characterized by probability density functions, which have been calculated on the basis of the real-world data and appropriate assumptions.[35,36] However, the overwhelming majority of the shale gas-based processes are designed to handle deterministic feedstock.[5,17-20,23,32,37] Existing studies typically assumed that the composition and supply can be perfectly known and fixed in advance without variability, which may lead to over-optimistic results and underestimation of the negative influences. For example, a mega-scale cracking plant can consume NGLs collected from hundreds of well-sites (rigs),[9,30] while

the raw gas composition and production rate of a single well-site keep fluctuating. If this plant is only designed to convert shale gas with a high NGLs content, the plant capacity is inevitably overestimated if the true composition deviates from the designed scenarios. To the best of our knowledge, the existing literature on addressing uncertainty in shale gas monetization processes primarily focused on the problems with a single or user-defined variability that creates a gap for their applicability. Gong et al.[9] developed a systematic simulation-based process intensification method for handling uncertain feedstock compositions in shale gas processing and NGLs recovery process systems. The uncertain set of compositions was derived from various shale plays and publications, instead of the field data from the same shale play. Wang and Xu[34] addressed the optimal design and synthesis of integrated NGLs recovery and LNG re-gasification under uncertain feed rates. They assumed a standard normal distribution for uncertain feed rates. Gao and You[38,39] addressed the optimal design and operation of shale gas supply chains under uncertainty using a scenario-based two-stage stochastic programming (SP) model. They used Monte Carlo methods to generate scenarios based on existing EUR data of 2,600 shale wells in Marcellus shale play.

Given the complex uncertain variability, a comprehensive systems design and analysis framework is required to decipher the true economic risk and environmental footprints of the shale gas monetization to the end-use products process under changing feedstock conditions and market fluctuations. To date, a number of research challenges in this field remain unsolved. These challenges include (a) how to simultaneously account for the mixed uncertainties, (b) how to incorporate real-world field data into the stochastic modeling, (c) how to develop efficient shale gas monetization pathways, (d) how to apply statistical techniques to rigorously interpret the risks. As will be shown, this article focuses on addressing these research challenges and develops a systematic monetization framework that incorporates stochastic

modeling and likelihood analysis of a large-scale shale gas to polymers process with consideration of endogenous and exogenous uncertainties.

Monetization Framework under Uncertainty

High pressure and gaseous crude mixture (>700 bar) extracted from a wellhead is first gathered at a nearby well-site where it first undergoes a remarkable pressure relief, causing a natural separation of raw gas from liquids (i.e. flow-back water and heavy hydrocarbons). Conventionally, depending on the wetness of the raw gas, the gas producer can either sell it to mid-stream companies by gathering pipelines or directly process it at a local processing facility. In the latter case, marketable NGLs separated from the PG are fractionated, stored, and then transported in a variety of forms like Y-grade stream, E-P mix and LPG stream.[40] Finally, the PG and NGLs purchased from mid-stream market hubs/centres are transformed into a number of value-added products in the downstream petrochemical enterprises.

In the newly-developed shale gas monetizing projects, the petrochemical facilities are co-located with shale plays and processing facilities. As shown in Figure 1, the entire project refers to a distributed-centralized conversion network considering the distributed gas processing, feedstock transportation, and centralized end-products production. The end-products investigated in this work include poly-propene (PP) and high-density polyethylene (HDPE). Herein, the first sub-step is to process raw shale gas through rejecting NGLs and undesired components (acid gases, water, etc.) in multi-site distributed processing facilities. The number of processing facilities depends on the capacity of each processing facility, polymers demand, and raw gas composition, etc. After that, the NGLs collected in a pooling system are moved to a centralized polymers production plant. Meanwhile, the lean gas can be used either as C_1 feedstock in the OCM reaction or, directly as marketable PG together with other processed

gases from the dry well-sites. Note that the utilization of dry gas is not considered in the scope of this research

This work proposes a systematic framework for monetizing raw shale gas to polymers and other by-products with consideration of complex uncertainty. In addition, this systematic framework is applicable to investigating the manufacturability of any other energy-chemical products. It involves a three-step statistical analysis as follows. *Step I*: it proposes a stochastic data processing strategy to characterize and quantify the endogenous uncertainties including gas composition and EUR associated with the feedstock acquisition. A finite size of scenarios is generated to accommodate the diverse nature of feedstock variability. *Step II*: The stochastic simulation requires a process model that can be evaluated under all generated scenarios to propagate the effects of feedstock variability. Herein, detailed distributed-centralized network systems of shale gas-to-polymers considering different monetization pathways are developed through rigorous process design, modeling and synthesis. Once all the scenario runs are completed, a set of model output variables of interest is mapped and collected. *Step III:* uncertain economic parameters extracted from the entire process are nested in the stochastic model to identify the probabilistic distributions and to perform a likelihood analysis of techno-economic-environmental objectives.

(Place **Figure 1** here.)

Proposed Approach

Step I: Feedstock variability quantification

Based on historical field data, in Figure 2 we combine three rigorous statistical methods, namely SAA, KSM, and DCSA, to characterize the significant variability in model input parameters in relation to uncertain gas composition and EUR. Scenario-based SP is a common

approach to explicitly account for uncertainties. However, due to the dependence of SP models on the scenarios, a large-scale shale gas project would involve raw materials collected from hundreds to thousands of shale wells, exponentially increasing the computational size and complexity. For instance, if we consider one hundred wells and each well has fifty independent initial production rates, fifty independent composition scenarios, and three independent well-refracturing operations, there will be $(50\times50\times3)^{100}$ scenarios in total. To obtain a manageable size, this study first indirectly addresses the high dimensionality and outliners of the original data. After that, SAA and KSM methods are mainly used to predict the minimum number of scenarios regarding the initial methane production rate and the corresponding initial production of other components, respectively. Finally, for each scenario, we normalize the gas composition and then estimate the EUR with consideration of well-refracture treatments using a DCSA method.

(Place **Figure 2** here.)

Four major assumptions considered in the data preparation model are made as follows. (1) For each generated scenario, the refracturing operations upon a well are less than three times;[10,12] (2) The raw gas composition of a sampling well remains unchanged throughout the lifespan and the trace impurities like O_2, He, Ar, and H_2O are not considered, that is, the raw gas only contains C_1, C_2, C_3, C_{4+}, N_2, CO_2, and H_2S;[9,30]; (3) The raw gas extracted from any shale well investigated is subjected to a classical Arps empirical decline curve;[41] (4) The production peak is independent of the timing of the well-restimulation operation.[10,12]

Sample Average Approximation

We are given a set of sampled wells and each well has known initial production rates of gas and tight oil (TO), as well as the raw gas composition being measured at the same production time and shale region. The outliers of sampled data should first be identified and

excluded from the original data by means of data diagnosis, thereby creating a new set of sampled wells (***I***). The corresponding initial gas production rate and components of a well belong to the sets $\boldsymbol{P} = [\, P_1^{t_0}, P_2^{t_0}, \cdots, P_I^{t_0}\,]^{\mathrm{T}}$ and $\boldsymbol{J} = [C_1, C_2, C_3, C_{4+}, N_2, CO_2, H_2S]$, respectively. In the process of reducing dimensionality, we first select the initial methane production rate of a sampled well *i* ($P_{i,C_1}^{t_0}$) as a sole objective value. Here, $P_{i,j}^{t_0}$ is a product of initial gas production rate of well *i* ($P_i^{t_0}$) and its concentration ($C_{i,j}$).

$$P_{i,j}^{t_0} = \boldsymbol{P} \times \boldsymbol{J}^{\mathrm{T}} = P_i^{t_0} \cdot C_{i,j} \tag{1}$$

We used an SAA method to generate a scenario set of $P_{i,C_1}^{t_0}$ to approximate the original expected objective value by calculating the sample average. The number of scenarios is determined by the desired level of accuracy of the solution, which can be measured by the confidence interval (δ) of the optimal solution. In this work, Oracle Crystal Ball is applied as a sample generator to obtain scenarios based on the Monte Carlo simulation method. As shown in Figure 2, we first solve the SP problem with a small number of initial sample size n_0 (i.e., n_0 = 50). Then, the Monte Carlo sampling variance estimator *var*(*n*) of the optimal solution for the SP problem, which is independent of the probabilistic distribution of the uncertain parameters, is provided by:

$$var(n) = \sqrt{\frac{\sum_{s=1}^{n} (\overline{P_{i,C_1}^{t_0}} - P_{s,C_1}^{t_0})^2}{n-1}} \tag{2}$$

where $n=n_0+\Delta n$; $\overline{P_{i,C_1}^{t_0}}$ and $P_{s,C_1}^{t_0}$ are the expected initial methane production rate of sampled wells and the initial methane production rate corresponding to scenario *s*, respectively. According to the central limit theorem, we use this sampling variance estimator to obtain the probabilistic distribution

$$P\left[\overline{P_{i,C_1}^{t_0}} - \frac{z_{\alpha/2} \cdot var(n)}{\sqrt{n}}, \quad \overline{P_{i,C_1}^{t_0}} + \frac{z_{\alpha/2} \cdot var(n)}{\sqrt{n}}\right] \geq 1-\alpha \tag{3}$$

where 1-α is the confidence level; $z_{\alpha/2}$ is the standard normal deviation such that 1-α/2 is subjected to a standard normal distributed variable $z \sim N(0, 1)$, $P(z \leq z_{\alpha/2})=1-\alpha/2$. For example, given a standard normal distribution with 95% confidence interval, we can refer to the distribution function tools and have $z_{\alpha/2}=1.96$. Given the $var(n)$ and the desired confidence interval δ_d, the minimum number of scenarios required can be determined by Eq. 4. Then, we update the sample size according to $n=n_0+\Delta n$, and solve the new SP problem again until the stopping criterion ($\delta \leq \delta_d$) is satisfied. The final optimal solution (N^*) can be regarded as a good approximation of the exact optimal solution of the original SP problem.

$$N^* = \left[\frac{z_{\alpha/2} \cdot var(n)}{\delta} \right]^2 \tag{4}$$

Kriging-based Surrogate Model

After the values of parameters N^* and $P_{s,C_1}^{t_0}$ ($s \in [1,2,\ldots, N^*]$) are obtained, the next step is to determine the corresponding initial production rate of other components. However, the sampling information of raw shale gas compositions might contain noisy data and is difficult to forecast, especially for the impurities and heavier hydrocarbons. Based on the sampled multi-well data, we develop a specialized surrogate model to approximate the true component distribution using the Kriging interpolation.[42-44] Specifically, this surrogate model is implemented by using the DACE (Design and Analysis of Computer Experiments)[45] toolbox in MATLAB that includes multiple sub-steps in series as shown in Figure 2. In each sub-step, we fit a single response surface (input-output variables) with respect to the original component distribution using field data. For example, in the sub-step S_5 the calculation ends by building an approximation model that is capable of linking the initial production rate of hydrocarbons (C_1~C_{4+}) with the initial production rate of acid gases. Each approximation model generally involves a regression term $f(\mathbf{x}, S_i)$ and a stochastic Gaussian process $z(\mathbf{x}, S_i)$, as given by:

$$y(\mathbf{x}, S_i) = f(\mathbf{x}, S_i) + z(\mathbf{x}, S_i) \tag{5}$$

where function $y(\mathbf{x}, S_i)$ is the response in sub-step S_i and $\mathbf{x}$ is the vector of k independent inputs. $f(\mathbf{x}, S_i)$ has polynomials of orders 0, 1, and 2. Usually an assumption of order =0 ($f(\mathbf{x}, S_i) = \boldsymbol{\beta}$) is sufficient for a good prediction, because $z(\mathbf{x}, S_i)$ can capture the significant behavior of y($\mathbf{x}$).[42] In sub-step S_i, the process covariance σ^2 for two inputs $\mathbf{x}^{\omega}$ and $\mathbf{x}^{\Psi}$ can be fitted by a spatial correlation function R ($I \times I$ matrix). In practice, R can be expressed by an exponential function, [46] in Eq. 6.

$$\mathbf{R}(\theta, \mathbf{x}^{\omega}, \mathbf{x}^{\psi}) = \prod_{h=1}^{k} \mathbf{R}_h(\theta_h \ \mathbf{x}_h^{\omega} - \mathbf{x}_h^{\psi}) = \prod_{h=1}^{k} \exp(-\theta_h \left| \mathbf{x}_h^{\omega} - \mathbf{x}_h^{\psi} \right|^{\theta_{k+1}}) \tag{6}$$

where $\theta_h \geq 0$ and $\theta_{k+1} \in [0,2]$ are adjustable parameters.

(Place **Figure 3** here.)

In each sub-step, the values of parameters σ^2, β, θ_h, and θ_{k+1} included in Kriging predictor are estimated by maximizing the logarithm of the likelihood of y($\mathbf{x}$). Detailed derivation can be found elsewhere.[42,45] Next, we sequentially add the new inputs ($\mathbf{x}^{\text{new}}$, $\mathbf{y}^{\text{new}}$) to the original data and calculate the generated augmented likelihood functions keeping the obtained parameters constant. The calculation sequence also follows the sub-steps shown in Figure 3, and in each sub-step a Kriging predictor given by Eq. 7 is applied. Note that, in this figure if the shale well investigated has the potential for oil production, we can also predict the initial tight oil production $P_{n,HC}^{t_0}$ in S_6 using the above mentioned method.

$$y(\mathbf{x}^{new}) = \beta^* + \mathbf{r}^T \mathbf{R}^{-1}(Y - \mathbf{1}\beta^*) \tag{7}$$

where

$$\beta^* = (\mathbf{1}^T \mathbf{R}^{-1} \mathbf{1})^{-1} \mathbf{1}^T \mathbf{R}^{-1} Y \tag{8}$$

$$\mathbf{r}(\theta, \mathbf{x}^{\omega}, \mathbf{x}^{new}) = \prod_{h=1}^{k} \mathbf{r}_h(\theta_h \ \mathbf{x}_h^{\omega} - \mathbf{x}^{new}) = \prod_{h=1}^{k} \exp(-\theta_h \left| \mathbf{x}_h^{\omega} - \mathbf{x}^{new} \right|^{\theta_{k+1}}) \tag{9}$$

where **r** (I×1 vector) is the correlation of sample points and new-added points, ω (ω=1, 2, ⋯, I), and Ψ (Ψ=1, 2, ⋯, I). Note that the accuracy of the KSM prediction can be captured by the mean-squared error (*MSE*) of the new input and sample point given by[45]:

$$MSE(x^{new})=\sigma^2[\mathbf{1}-\mathbf{r}^T\mathbf{R}^{-1}\mathbf{r}+(\mathbf{1}-\mathbf{r}^T\mathbf{R}^{-1}\mathbf{r})^2/\mathbf{1}^T\mathbf{R}^{-1}\mathbf{1}] \quad (10)$$

Integrated Decline-Stimulate Analysis Curve

The gas production rate of a well exhibits a characteristically hyperbolic decline curve during its lifespan due to the inherently low permeability and pressure depletion of the shale reservoirs. Well-refracturing is a newly-developed process which presents a promising strategy for addressing this steep decline rate of a developed well. To capture the complex competing effect, an integrated DSAC model integrating Arps decline formula and refracturing formula is developed to quantitatively estimate the EUR under uncertainty. In this model, the original decline curve of production rate that exhibits a hyperbolic trend in the production reduction is described by a widely-accepted Arps decline formula given in Eq. 11.[41,47]

$$P_s^t=\begin{cases}0 & t\in(0,t_0)\\ P_s^{t_0}\cdot\left[1+b\cdot D_i(t-t_0)\right]^{-1/b} & t\in[t_0,T_{ls}]\end{cases} \quad (11)$$

where T_{ls} is the expected productive lifespan of the investigated shale well; D_i (>0) and b (>1) are the initial decline rate and decline exponent; t=0 and $t=t_0$ correspond to the start dates of the completion operation and gas extraction, respectively. Normally, t_0 is no longer than two months (i.e., t_0=1).

When the operation of multiple refracture treatments is implemented, the productivity can be further expressed using discrete-time and multi-period functions as follows:

(1) Initial fracturing and production period:

$$P_s^t=\begin{cases}0 & t\in(0,t_0)\\ P_s^{t_0}\cdot\left[1+b\cdot D_i(t-t_0)\right]^{-1/b} & t\in[t_0,trt_1]\end{cases} \quad (12)$$

where *trt* (in months) is the timing of the refracture treatment, and trt_1 is the start date of the first refracturing. The proper time for refracturing is when the gas production drops to less than 15% of the original value, indicating that $(1+ b\cdot D_i\cdot trt_1)^{-1/b}\leq 0.15$.

(2) The first refracturing and production period:

$$P_s^t = \begin{cases} 0 & t \in (trt_1 + drt, trt_1 + drt + 1] \\ \gamma \cdot P_n^{t_0} \left[1 + b \cdot D_i (t - t_0)\right]^{-1/b} + \beta_1 \cdot P_n^{t_0} \times & \\ \left[1 + b \cdot D_i (t - trt_1 - drt)\right]^{-1/b - \phi \cdot trt_1} & t \in (trt_1 + drt + 1, trt_2] \end{cases} \tag{13}$$

where *drt* is the duration of refracturing treatment; γ, β_1, and ϕ are coefficients that account for the contribution of initial fracture, first peak reduction ratio of post-refracturing, and the increase in the steepness of decline after refracturing, respectively; and $trt_2 = trt_1 + drt + 1 + \Delta t_1$, herein Δt_1 is the production interval after the first refracturing. Note that, in Eq. 13 we assume that the steepness of the productivity declines after refracturing increases linearly with the time interval between the initial completion and the current refracturing operation. In addition, the resulting production peak is independent of the timing of the well-restimulation indicated in the works of Cafaro et al.[10] and Tavassoli et al.[12]

(3) The m^{th} ($1<m\leq M$) refracturing and production period:

$$P_s^t = \begin{cases} 0 & t \in (trt_m + drt, trt_m + drt + 1] \\ \gamma \cdot P_s^{t_0} \left[1 + b \cdot D_i (t - t_0)\right]^{-1/b} + \beta_m \cdot P_n^{t_0} \times & \\ \sum_{\tau=1}^{m} \left[1 + b \cdot D_i (t - trt_\tau - drt)\right]^{-1/b - \phi \cdot trt_\tau} & t \in (trt_m + drt + 1, trt_{m+1}] \end{cases} \tag{14}$$

where $trt_m = trt_1 + drt\sum_{\tau=1}^{m}(\tau - 1) + m + \sum_{\tau=1}^{m}\Delta t_{\tau-1}$ and $b\neq(1-\phi\cdot trt_m)^{-1}$ for the last production period (m=M), and the boundary constraint is $trt_M + drt + \Delta t_M = T_{ls}$.

To estimate the EUR, the cumulative production of shale gas extracted that can be calculated using distributed definite integral from time t=0 to time $t=T_{ls}$, is given in Eq. 15.

$$EUR_s = \int_0^{T_{ls}} P_s^t dt = P_s^{t_0}\left[D_i\left(b-1\right)\right]^{-1}\left[\left[b\cdot D_i\cdot\left(trt_1 - t_0\right)+1\right]^{1-1/b} - 1\right]$$
$$+\sum_{m=1}^{M}\beta_m\cdot P_s^{t_0}\left[b\cdot D_i\left(-1/b-\phi\cdot trt_m+1\right)\right]^{-1}\left\{\begin{array}{c}\left[1+b\cdot D_i\cdot(\Delta t_m+1)\right]^{-1/b-\phi\cdot trt_m+1}\\ -\left[1+b\cdot D_i\right]^{-1/b-\phi\cdot trt_m+1}\end{array}\right\} \quad (15)$$
$$-\sum_{m=1}^{M}\gamma\cdot P_s^{t_0}\left[D_i\left(b-1\right)\right]^{-1}\left\{\begin{array}{c}\left[b\cdot D_i\cdot\left(trt_m+drt+1\right)+1\right]^{1-1/b}\\ -\left[b\cdot D_i\cdot\left(trt_{m+1}\right)+1\right]^{1-1/b}\end{array}\right\}$$

Another goal of this step is to classify the shale wells into wet and dry by checking the raw gas quality in each scenario. If it meets the specification of high heating value (S_{hhv}), this shale gas well would be considered as a wet well from which the extracted raw gas is suitable for the downstream monetizing technologies employed in this work; otherwise, we consider that it has low potential for chemical production because it produces raw gas with low NGLs content. Thus, we only focus on the resulting subset of scenarios in relation to the wet wells ($N^{\dagger}$, $\leq N^*$) in the next steps.

Step II: Process Modeling and Synthesis

In this sub-step, as mentioned before, the feedstock variability is propagated through performing a detailed process modeling method on distributed-centralized conversion network systems. The process unit models are mainly solved in ASPEN HYSYS expect the olefins polymerization unit, which is realized by ASPEN PLUS.

Distributed shale gas processing

The multi-site distributed processing facility mainly includes sweetening, dehydration, and NGLs cutting units.

Gas Sweetening

Modeling a gas sweetening unit involves the determination of an efficient purification approach for the raw shale gas in order to meet the equipment and pipeline specifications. Specifically, the H_2S and CO_2 concentrations of sweet gas should ideally not exceed 4.0 ppm

and 2.0 mol% to avoid potential corrosion and freezing problems, respectively.[48] Figure 4(A) illustrates three technological alternatives[49] considered in this model as follows: (a.1) for a low H_2S concentration (<4.0 ppm), a fixed-bed type scavenger process is a cost-effective approach to H_2S removal; (a.2) for moderate CO_2 (>2.0 mol%) and H_2S concentrations (<4.0 ppm), the absorption-based acid gas removal (AGR) process followed by a scavenger process works well; and (a.3) for a moderate to high H_2S content (>4.0 ppm), a sulfur recovery process combined with an AGR process is necessary since the sulfur must be captured if its amount exceeds the limit specified by the environmental regulations.

(Place **Figure 4** here.)

The AGR process mentioned in the last two cases usually employs an absorber-stripper configuration where acid gases are dissolved in a lean solvent like diethanolamine (DEA) by the absorber, and then are released in the overhead gas by the stripper. However, the rejected acid gas has a low H_2S content and a high CO_2/H_2S mass ratio, making it unsuitable for sulfur recovery directly using the traditional Claus process.[50] An acid gas enrichment (AGE) process using a selective solvent such as methyl-diethanolamine (MDEA) is able to increase the H_2S content in acid gas by absorbing the H_2S and allowing about 80% of the rejected CO_2 to remain in the CO_2 slip.[51] The enriched acid gas enters a Claus section in which one third of H_2S is oxidized to SO_2 by a slight excess of air. The generated SO_2 further reacts with the H_2S in the by-passed acid gas to yield sulfur. After that, a Shell Claus Off-gas Treating (SCOT) process including a hydrogenerator, quench column, absorber, and incinerator is adopted to essentially convert the remaining sulfur compounds in Claus tail gas to H_2S. Finally, the rich solvent exiting from the SCOT absorber is recycled to the AGE stripper for solvent generation.

Dehydration and NGLs Cutting

In Figure 4(B), hydrate formation and equipment corrosion potentially occur in a moist environment. To remove the moisture from the sweet gas, a dehydration process using triethylene glycol (TEG) is employed. Similar to the AGR process, an absorber-stripper configuration is employed, and the sweet gas first flows into a TEG contactor where it is counter-currently dried by a rich TEG solvent. The TEG-rich solvent leaving from the contactor bottom flows through a TEG till to regenerate the solvent. The dry gas with 0.1 ppm moisture from the contactor top is introduced to an NGLs cutting section in which a typical turbo-expansion configuration combined with an external refrigerant is adopted to recover about 80% of the ethane and 99.9% of the methane from the incoming gas.[30,52] The recovered NGLs from the demethanizer bottom is pumped to the downstream centralized plant. Meanwhile, a small fraction of lean gas (<0.1%) is used as stripping gas in a modified surge tank, lowering the water concentration in the lean TEG stream from 1.0-5.0 wt% to less than 0.3 wt%. The remaining lean gas exiting from the contactor top is either pipelined to the centralized plant as C_1 feedstock, or compressed to 70 bar and directed to the gas pool as saleable PG.

Centralized polymers production

For the last sub-step, either the hybrid methane and NGLs or solely the NGLs are converted to polymers in a centralized production plant, resulting in two monetization pathways termed hybrid pathway and NGLs pathway. The first pathway includes five process units (mixture fractionation, H_2/olefins recovery, C_2-C_3 pyrolysis, C_1 pyrolysis, and CO_2 capture and storage) and a utility facility. While the last two process units, namely C_1 pyrolysis unit and CO_2 capture and storage unit, as well as the syngas separator in C_2-C_3 pyrolysis unit, need to be eliminated in the second pathway due to the absence of C_1 conversion. Details are introduced as follows.

Mixture Fractionation

The pipelined NGLs can be separated into a series of hydrocarbons by a fractionation train in a typical natural gas refinery. Meanwhile, we note the cracking gas contains very similar components compared with the OCM product. Based on a heuristic method for synthesis of the distillation sequence, it has recently been pointed out that they can be cost-effectively co-processed using a complex separation strategy, which leads to better energy saving and equipment-sharing opportunities.[17,34] The fractionation train is designed to sharply separate the heavier hydrocarbons (ethylene, ethane, etc.) from non-hydrocarbon components like syngas in the incoming gas. More specifically, ethane+, propane+, and butanes+ included in the incoming gas are sequentially separated through passing through a series of cryogenic distillations that consisted of demethanizer, deethanizer, and depropanizer, respectively, as shown in Figure 5(A).

(Place **Figure 5** here.)

H_2/Olefins Recovery

The process H_2 and olefins can be simultaneously recovered in this unit where a syngas separator is first used to reject H_2-rich non-hydrocarbons from the light fraction at the top of the demethanizer. The overhead from the syngas separator contains around 60 mol% H_2, which can be directly used as the furnace fuel or for H_2 production. The bottom liquid of the demethanizer essentially contains methane which can be used as the OCM feedstock after cooling heat recovery and expansion. In this model, we consider a zero H_2 output scheme in which a certain portion (50~70%) of this H_2-rich gas is charged to power plant in a utilities facility as gas turbine (GT) furnace fuel. This is because a zero H_2 output scheme would be self-sufficient in terms of energy and emit much less process GHGs, as supported by our previous work.[30] The remaining H_2-rich gas is purified via a common pressure swing adsorption (PSA) process to meet the requirement of process H_2. This PSA block is modelled

using a component separator that recovers 90.0% of the industrial-grade H_2 (99.5 mol%) at 24.9 bar. After leaving the PSA block, the pure H_2 is used to hydrogenate sulfur dioxide (see Figure 4(A)) and acetylene (see Figure 5(B)), as well as to dilute the reactants of polymerization in Figure 7(F). The PSA tail gas is discharged at 1.5 bar and also sent to the GT furnace.

The C_3 fraction split from the depropanizer top (see Figure 5(A)) is fed to a C_3 splitter modelled as a heat-integrated distillation column which can efficiently recover the propylene product at polymer grade (99.5 wt%). Meanwhile, the deethanizer top product, C_2 fraction, goes to a front-end hydrogenator to essentially eliminate the tiny bit of acetylene. Then, a C_2 splitter separates the hydrogenator effluent into three products as follows. The overhead product, C_1 residue, containing small amounts of methane is sent to the C_1 pyrolysis unit. The side-draw liquid is polymer-grade ethylene at 99.9 wt% that is used as the polymerization feedstock. The bottom liquid containing ethane at 98.0 wt% is fed to a C_2 cracker in the following paraffin pyrolysis unit as the raw material.

Paraffin Pyrolysis

In Figure 4, the lean gas stream pipelined from a gas pooling system is divided into two branches. The upper branch is used as the cracking fuel. The lower one has two purposes as follows (i) directly compressed to 70 bar as the saleable PG; (ii) depressed to 2.0 bar and then mixed with O_2 at O_2/CH_4=0.65 on a molar basis. In the latter case, the mixture is pre-heated and sent to a fixed-bed OCM reactor with La_2O_3/CaO catalyst.[53] The reactor modelled as an isothermal CSTR with an exterior cooling wall operates at a pressure of 1.6 bar, at a temperature of 800^{o}C. This reaction scheme has three primary and seven consecutive reactions, as listed in Table S-1 in the Supporting Information (SI). The reactor effluent is cooled to 100^{o}C and then quenched to 35^{o}C by cooling water. Next, the dehydrated OCM product is compressed to 30 bar, and finally sent to an AGR section in the CCS unit for CO_2 sequestration.

(Place **Figure 6** here.)

Air is first compressed to 13.1 bar via a four-stage main air compressor, and then sent to a cryogenic distillation system modelled as a component separator where the following assumptions on design have been made:[5] O_2 is recovered at 10.0 bar and 32.0°C with component recovery rates of O_2, N_2 and Ar, as 0.94, 0.005, and 0.704, respectively; HP N_2 is recovered at 12.6 bar and 10.0°C with component recovery rates of O_2, N_2 and Ar, as 0.002, 0.119, and 0.024; low pressure (LP) N_2 is recovered at 3.9 bar and 32.2°C with component recovery rates of O_2, N_2 and Ar, as 0.015, 0.736, and 0.146; and the remaining stream is waste gas and discharged at 1.1 bar. The total ASU power requirement (W_{ASU}) can be approximated by[54]:

$$W_{ASU} = W_{aircomp} \times \left(0.550 \times C_{O_2} + 0.478\right) \tag{16}$$

where $W_{aircomp}$ is the net power consumption of the main air compressor (MWh), and C_{O2} is the O_2 molar purity (%). A small amount of O_2 (0.5-2.0%) is used for the Claus process. Meanwhile, about 50-90% of HP N_2 is split and sent to the GT combustor and the PP production section. The remaining HP N_2 is expanded through turbines to recover mechanical energy and then vented to the atmosphere with the LP N_2.

As shown in Figure 5(C), C_2-C_3 pyrolysis involves cracking of ethane and propane in parallel into ethylene and propene, respectively. In industry, the two hydrocarbon cracking facilities are both mainly installed with a pre-heating/mixing zone and a reaction zone. In the first zone, the feedstocks are diluted with medium pressure steam (MPS) and hydrogen to 0.4 kg/kg ethane and 0.6 mol/mol propane, respectively, and pre-heated to their reaction temperatures. The diluents can reduce the partial pressure of paraffin in the gas phase and inhibit coke formation. After that, the reactants enter the reaction zone where the molecules of ethane and propane are mainly dehydrogenated into olefins and other by-products. Note that the two dehydrogenation reactions are highly endothermic. The ethane cracker based on a common steam cracking technology is simulated using a three-stage Plug Flow Reactor (PFR)

with specified external heats. Meanwhile, modeling of the propane cracker based on UOP-Olefiex technology[55] is implemented using a four-stage adiabatic PFR supported by inter-stage heaters among each PFR. The crackers are both integrated with radiation burners located in the side walls of the fired furnace, and the heat required is fully provided by the combustion of external methane. The kinetic reaction schemes of ethane cracking and propane cracking are taken from the literature[56-58], and the details of kinetic equations and parameters are given in Tables S-2 and S-3 in SI. The reactor effluents can be preliminarily processed via multiple steps (cooling, compression, dehydration, and purification), and finally flow to the mixture fractionation unit.

CO_2 Capture and Sequestration

CCS operation becomes a key approach to reduce process CO_2 emission, as well as the global warming potential (GWP).[59] Typically, a CCS operation mainly includes CO_2 absorption, dehydration, CO_2 compression and transportation, as well as CO_2 injection.[60] In this study, the GWP mitigation opportunity comes from the implementation of CCS operation for the CO_2 vapor (see Figure 6(E)) derived from the OCM reaction. This stream contains around 90 mol% CO_2 and 10 mol% H_2O, indicating that an energy-intensive CO_2 absorption process can be eliminated. Note that the CCS operation of flue gases from the GT furnace and cracker furnace are not considered. This is primarily due to their low CO_2 concentration (< 10 mol%) which causes a high energy penalty for the CCS operation. In order to be ready for sequestration, the removed CO_2 must first be compressed into the liquid phase at 80 bar through a middle pressure (MP) compressor followed by a HP compressor. Note that an inter-stage TEG dehydration is required to dehydrate the MP CO_2 stream. The CO_2 liquid is pumped at 153 bar, which is a supercritical pressure suitable for distribution in the CO_2 pipeline. The recovered CO_2 has a high purity (>99 mol%) with sufficiently low impurities that meets NETL specifications[61].

Olefins Polymerization

(Place **Figure 7** here.)

The olefins (ethylene and propene) recovered from the H_2/Olefins recovery unit in Figure 5(B) are polymerized to long-chain polymers, namely HDPE and PP. As shown in Figure 7(F.1), the incoming ethylene, together with solvent (n-C_6H_{14}), is compressed to 200 bar via a high-pressure pump. The mixture is then split into two branches. The upper branch making up 66.6% of the total is charged to a fixed-bed reactor (FBR I, modelled as a CSTR block). A high molecular weight polymer can be generated at 160^{o}C using two-site Ziegler-Natta catalysts including $TiCl_4$ and $C_6H_{15}Al$.[62] The POLYPCSF property method[62] with supplied parameters for catalysts is employed to describe the behaviour of gaseous components consisting of N_2, H_2, C_2H_6, and C_2H_8. The effluent of FBR I, together with the lower branch of mixture, is introduced to FBR II where a relatively high molecular weight polymer is generated. Note that in the polymerization of ethylene, H_2 is used as a chain transfer agent to control molecular weight. Unreacted monomers, solvent, and H_2 are recycled through a high pressure flasher (HPF, 30 bar) followed by a low pressure flasher (LPF, 1 bar). HDPE product is recovered at 99.1% mass purity, and its average density, poly-dispersity index (PDI), and average segment molecular weight (MW_{SEG}) are 0.955 g/cm^3, 3.61, and 28.05, respectively.

A gaseous UNIOPL process is employed for the homo-polymerization of PP, as depicted in Figure 7 (F.2). The major feedstock, propene, is diluted with inert (C_3H_8 and N_2) according to the mass ratio of inert and propene equaling 0.009:1.[62] After that, the mixture, together with catalysts ($TiCl_4$ and $C_6H_{15}Al$), inert gas (C_3H_8 and N_2), and chain transfer agent (H_2), is co-fed to a fluidized-bed reactor (FBR). The FBR operating at around 70^{o}C and 28~30 bar is simulated using a single CSTR block with a multi-site Ziegler-Natta kinetic model.[63] The POLYPCSF property method[62] is also employed to describe the behaviour of gaseous components

consisting of N_2, H_2, C_3H_8, and C_3H_6. The vapor effluent of FBR is condensed and then recycled to the FBR. The bottom effluent of FBR containing PP and inert gas can be purified by passing through a flasher operating at 5.0 bar, followed by a stripper with N_2 as stripping gas operating at room conditions. The average density, PDI, and MW_{SEG} of PP product are 0.920 g/cm^3, 4.55, and 42.08, respectively. Note that the purified polymers finally need to be processed by dry granulators in practice.

Utility Facility

The power, heat, and mass integration of the process are carried out aiming to reduce utility consumption. All process waste streams such gas PSA tail gas are mixed and diluted to 122 Btu/scf in LHV with N_2 from ASU. The diluted mixture is charged to the GT combustor followed by expanders for shaft work generation. The thermal energy of GT effluent is further recovered by the steam turbine and heat recovery steam generator. Once the process waste stream is exhausted, a mixed integer linear programming model is implemented to design the optimal heat exchanger networks. The utilities facility also includes a wastewater treatment (WWT) section that mainly consists of the multi-effect distillation (MED) and total dissolved solids removal. Following the work of Gabriel et al.[64] and Martínez et al.[65], a simple direct recycle strategy is established for reducing water consumption and discharge. The direct recycle strategy is complemented by taking into account the water impurities of all potential sources and allowed water impurities of the potential sinks. In particular, this study considers that the blowdown from the quench column (see Figure 5(C)) contains minimal total dissolved solids (TDS), oxygenated compounds (CO and CO_2), and hydrocarbons. The MED generated water is sent directly to the TDS removal unit where the discharged water must meet the appropriate quality specifications[48] (see Table S-4 in SI) for the usages of cooling water and boiler feed water.

Feedstock transportation

This work considers the utilization of pipeline networks as the major conveyance. To estimate the transportation distance, we consider the distributed processing facilities located in a hypothetical square area. The average delivery distance ($\overline{d_p}$) of raw gas from the well-site to a processing facility is equal to the average distance from a random point in the square to the center of the square, as shown in Eq. 17.

$$\overline{d_p} = \pi \sqrt{\frac{q_p}{Y_{rg} f}} \int_{-0.5}^{0.5} \int_{-0.5}^{0.5} \sqrt{x^2 + y^2}\, dx dy = 0.383 \times \pi \sqrt{\frac{q_p}{Y_g f}} \tag{17}$$

where π is the terrain factor (≥1, assumed to be 1.2 on average[27,28]), which is a function of a region's pipeline network development and reflects the ratio of actual distance to the ideal straight line distance to a processing facility. q_p, Y_{rg}, and f are the capacity of the processing facility, raw gas extraction per square mile, and the ratio of wet wells to total wells, respectively. Once the raw shale gas is processed, the next stage is to collect and move the resulting gas/liquid streams to the centralized plant. The corresponding average pipeline distance ($\overline{d_c}$) between the distributed processing facility and the centralized polymers production plant can be estimated by an empirical formula[27] provided by:

$$\overline{d_c} = \pi \cdot \mu \cdot \sqrt{\frac{q_c}{Y_{wg} f}} \left(\frac{q_p}{q_c}\right)^{\nu} \tag{18}$$

where q_c and Y_{NGLs} represent the capacity of the polymers production plant and wet gas extraction per square mile; μ and ν are empirical coefficients.

Tables S-5~S-9 in SI lists the pipeline size, average area of a shale well, and other coefficients. This information can be further used to estimate the total pipeline lengths and transportation costs of lean gas and NGLs shipped to the polymer production plant.

Step III: Likelihood Estimation

Based on the two above steps, we obtain a stochastic model with a finite number of independent scenarios ($N^{\dagger}$). For each scenario, the model outputs including plant-level yields, consumptions, equipment sizes, and emissions are known perfectly in the previous step. In this step, a set of independent economic parameters extracted from the entire process is nested in this stochastic model. In particular, each economic parameter is assigned a certain type of probability distribution. As shown in Figure 8, the Monte Carlo simulation method is used to perform the uncertainty analysis of economic parameters. The values of varying economic parameters are sampled randomly from the user-specified probabilistic distribution. In this way, for each scenario, a set of resulting outputs (sub-scenarios, N^{+}), with respect to the process performances, is recorded by conducting a sufficient number of sets of samples. If we further consider all scenarios and their samples, a large-scale "pool" of sub-scenarios ($N^{\Theta}=N^{\dagger}\times N^{+}$) resulting from hundreds or thousands of sets of samples will be gathered for the likelihood analysis. Thus, we can identify the probability distributions and then estimate the max-likelihood estimation (MLE) of project performance objectives as follows:

(Place **Figure 8** here.)

One major objective of this work is to investigate the financial risk of the shale gas monetizing project over its lifespan, which can be measured by the levelized production cost of PE (LCOP, $/ton). This performance indicator can be represented as:

$$\text{LCOP}=\frac{\text{Life cycle cost}}{\text{Lifetime polymer production}}=\frac{TPC+\sum_{t\in T_{ls}}\left[\frac{AF+AO}{(1+DR)^{t}}-\frac{RV}{(1+DR)^{t}}-\frac{\sum_{bp}R_{bp}}{(1+DR)^{t}}\right]}{T_{ls}\times AP_{\text{PE}}} \quad (19)$$

where AF, AO, and AP_{PE} are annualized parameters including the feedstock cost, operating cost, and production amount of PE, respectively; TPC, DR, RV, and R_{bp} are the total project cost, discount rate, residual value, and the revenue by selling by-product bp. In the calculation of

LCOP, we consider that the raw shale gas is directly purchased from the raw shale gas producer at its real extraction cost instead of the market price. The extraction cost of shale gas at the wellhead is highly correlated with the investment and EUR which can be measured by the breakeven gas price (BEGP, $/mmbtu) using a full-cycle per-well (FCPW) approach.[66,67] The investment includes the costs for drilling and completion, leasing of acreage, refracturing, operations and maintenance, payment of royalties and taxes; they are all on the individual scenario (well) basis.

A gate-to-gate boundary of the environmental analysis is used to measure the plant-level GWP for manufacturing l ton of PE, which is a relative measure of how much radiated heat is trapped by emissions of GHGs = [CO_2, CH_4, SO_2, and NO_x] in the atmosphere over a specific time interval. That is, the GWP calculation given by Eq. 20 focuses on the global warming effects caused by GHGs.

$$GWP = \frac{AT \times (\sum_{g \in \mathrm{GHGs}} \sum_{v \in \mathrm{WS}} MF_v \times WF_g \times \varphi_{g,gwp} + \sum_{u \in \mathrm{U}} CR_u \times \lambda_{u,CO_{2-eq}}) \times \eta_{PE}}{AP_{PE}} \quad (20)$$

where AT is the annual operating time; MF_v and WF_g are the mass flow rate of the waste stream v and the weight fraction of the discharge g; CR_u is the consumption rate of the utility u; $\varphi_{g,gwp}$ is the damage factor which accounts for the GWP associated with the discharge g relative to that of CO_2; $\lambda_{u,CO_{2-eq}}$ is the amount of equivalent CO_2 emissions associated with the consumption of u; η_{PE} is the economic value-based allocating factor which reflects the contribution of PE production to the total GHG emissions. These data are updated from publications, GREET[68] and Ecoinvent[69] databases, as listed in Table S-10 in SI.

Illustrative Examples

The proposed shale gas monetization framework is applied to four distinct case studies including two sets of influencing factors as follows. (1) Plant location: feedstock is collected

from two shale regions, namely the Appalachians (AP, includes Marcellus, Big Sandy, etc.) and the Gulf Coast (GC, includes Eagle Ford, Haynesville, etc.); (2) monetization pathway: end-use products can be manufactured via either only an NGLs pathway design or a combination of C_1 pathway design and NGLs pathway design. Thus, these examples will be denoted by AP-O, AP-H, GC-O, and GC-H where AP and GC denote the plant located in the AP and GC regions, and O and H denote polymers which are derived from NGLs only (O) and hybrid NGLs and methane (H). The distributed processing facility and centralized production plant are considered at 50 mmscfd of raw gas input and 300 kton per year of polymers production. Besides, allowable by-products consist of PG, butanes+, sulphur, and electricity.

The basic field data that includes site name, well number, age, wellhead pressure, water and carbon footprints, extraction rates of raw gas and tight oil, as well as gas composition are mainly derived from on-site measurement and statistics by Allen and co-workers,[47,70] as given in Table S-11 in SI. In particular, a total of 162 shale wells from 45 production sites in the AP shale region which reported natural gas production were measured, while in the GC region the measured data came from 146 shale wells (58 well-sites) with co-production of gas and tight oil. The general assumptions and default operating conditions used in the process simulation are summarized in Table S-12 in SI. Detailed capital cost parameters used in the LCOP calculation are given in Table S-13 in SI. Besides, in the step of likelihood estimation, twelve assumptions that include investment, products, electricity, and refrigerant prices are specified in Table 1. Each selected assumption is assigned a range of values and a uniform distribution based on market values in recent years. Besides, the triangular distributions of TPC ranging from ±25% of the deterministic values are assumed in the likelihood estimation model.

(Place **Table 1** here.)

Result and Discussion

The proposed strategy and models were realized by combining ASPEN HYSYS (PLUS) V7.2 and MATLAB R2010a. This work employed a customized MATLAB-ASPEN interface[5] to collect, map, and process the uncertain input-output information which was carried out on a workstation with an Intel Four-processor Xeon E5 CPU@2.5 GHz and 32 GB RAM. The calculation time for each computational case study ranged from 3-12 hours mainly depending on the scenario size (that is $N^{\dagger}$) generated by the SAA method. An in-depth discussion of the uncertain parameters and techno-economic-environmental results are presented as follows.

Uncertain Parameters

The outliers of field data regarding the initial gas production rate are identified and excluded using box-and-whisker diagrams, and the corrected boxplots are also presented in Figure 9(A). Through considering a 95% confidence interval, the scenario sizes are finalized as 200 and 250 for the projects located in the AP and GC regions, respectively, using the SAA method. Meanwhile, we measure the frequency histogram of $P_{s,C_1}^{t_0}$ shown in Figure 9(B), which can be assumed to follow the lognormal distribution for the AP region case and the Beta distribution for the GC region case recommended by the Anderson-Darling test.[71] In this figure, a comparison between the $P_{s,C_1}^{t_0}$ distribution derived from field data and that from the proposed SAA method indicates that the SAA method can provide a good approximation. Based on the approximation of sampled data, the KSM method is applied to successively predict the initial production rate of other components. Figure A-1 in the Appendix compares the predicted mesh plot/value and sampled data. As shown, all functions are fit to an accuracy of $\overline{MSE}$ (mean value of MSE) <5, indicating that confident predictions are obtained.

(Place **Figure 9** here.)

(Place **Figure 10** here.)

For a given gas feedstock, as we know, a higher heating value generally means that it contains a higher NGLs content and lower impurities content. For all scenarios considered, we first use the HHV distribution of shale gases to illustrate the effect of compositional uncertainty, as shown by the colored dots in Figure 10(A). The green and blue lines represent the mean values of HHVs (M_{hhv}), which are 1,018 btu/scf and 1,101 btu/scf for the AP and GC regions, respectively. From the comparison of HHVs, it is statistically proved that the type of raw gas produced from the AP region is fairly stable and dryer than that of the GC region in terms of the NGLs content. Figure 10(B) rearranges the results of the green and blue dots to present the corresponding cumulative possibility distribution. The estimated HHVs of shale gas produced from the AP and GC regions range from 1,022 to 1,190 btu/scf and 1,021 to 1,420 btu/scf, respectively. Considering the requirement for raw gas quality (S_{hhv}), this study specifies the NGLs concentration to be less than 3 mol% (after gas sweetening), and the corresponding minimum HHV is 1,028 btu/scf. Thus, for both shale regions, the mean values of raw gas HHV are lower than this requirement. Especially, for the AP shale gas, only 0.08% of scenarios ($N^{\dagger}$=30) are eligible to be selected. As for the GC shale gas, this ratio goes up to 46.4% ($N^{\dagger}$=116). In the process of scenario selection, it is impressive to see that the median of the initial production rate of the AP shale gas increases remarkably from 0.198 to 0.237 bscf/(mon·well), while this value for the GC shale gas declines from 0.187 to 0.159 bscf/(mon·well). Meanwhile, the mean value of the HHVs increases to 1,043 btu/scf for the AP shale gas and 1,183 btu/scf for the GC shale gas.

(Place **Figure 11** here.)

For all scenarios selected above, Figure 11 shows the representative production rate in terms of $\overline{P_{N^{\dagger}}^{t_0}}$ within its lifespan using the DCSA method. The effects of important uncertain factors including production decline and refracture operation are also presented in this figure.

The first peak of the production rate represents the average level of the initial production rate ($P_n^{t_0}$) which is 246 mmscf/(mon·well) for the AP region and 132 mmscf/(mon·well) for the other. Accordingly, when the well-restimulation is not taken into account (M=0), the resulting gas EURs of the AP and GC shale regions are 6.69 bcf/well and 3.18 bcf/well, respectively. Note that these observations are not consistent with our previously determined predictions[30] where the expected gas EURs of the two regions are 0.97 bcf/well and 3.49 bcf/well. The current prediction provides a more confident result since it is derived from the rigorous statistical analysis of actual data, and exactly reflects the diversity of the shale resources investigated. Figure 11 also shows the results of well-restimulation over the lifespan of representative wells. As shown, the shale operator in the AP region can boost the mean value of gas EURs from 6.99 bcf/well to 8.62 bcf/well for only a single refracture treatment. This number continues to increase to 8.90 bcf/well for a double treatment and 9.10 bcf/well for a triple treatment. Likewise, in the GC shale region, the mean value of gas EURs can be maximized to 5.40 bcf/well when the well is restimulated three times over its lifespan. In summary, the results show that the refracture treatment would lead to a remarkable increase in the expected gas EUR by 25-39% over the given planning horizon.

Plant-level Model Outputs

For a better comparison, this section focuses on analyzing the outputs of techno-economic analysis according to the representative production rate shown in Figure 11. Table 2 summarizes the results of transportation, feedstock, utility, yield, emission, and capital cost for all the four case studies evaluated. As listed in this table, the feedstock supply of the proposed distributed-centralized network system involves thousands of shale wells, tens of processing facilities, and hundreds of miles of the total gathering pipeline. For given capacities of processing and production, the number of processing facilities depends on the joint effects of feedstock quality and gas EUR (production rate). Relatively, the monetizing projects fed by

NGL-rich feedstock such as GC shale gas consume less raw shale gas, lowering the carbon input and the number of processing facilities and shale wells. Taking the NGLs pathway design as an example, manufacturing 300 kton of polymers (HDPE + PP) per year from the GC shale gas consumes 62.5 ton/h NGLs as the immediate, corresponding to a total NGLs output of 3 processing facilities. The number of processing facilities significantly increases to 23 if the feedstock is switched to the AP shale gas under the same design. On the other hand, the GC shale wells suffer lower EURs, inevitably requiring more shale wells and longer pipeline distances. It should be noted that the hybrid pathway design can lead to a reduction in the number of required processing facilities, especially for the project fed by the NGLs-lean feedstock. Furthermore, given the processing capacity of 50 mmscfd, this design significantly decreases the total capital cost of processing facilities in the AP shale region from $443MM for the AP-O case study to $108MM for the AP-H case study, indicating a 75% drop.

(Place **Table 2** here.)

As listed in Table 2, the manufacture of polymers is quite energy intensive, resulting in a high specific energy consumption that ranges from 165-200 GJ per ton for the AP shale gas and 116-160 GJ per ton for the GC shale gas. To maintain the same plant capacity, the monetization process driven by NGL-lean shale gas co-produces significantly more PG and butanes+ by using more process utilities compared with the case of NGL-rich shale gas. Note that the centralized production plants have been energy-optimized such that in an extreme case study of the AP-H, the overall process becomes a net exporter of surplus electricity. Another fundamental reason lies in the great amount of power generation in this case through recovering the excessive high-temperature heat discharged from the OCM reaction. Besides, Table 2 shows the hybrid pathway design that uses a CCS operation is capable of essentially capturing

the OCM-derived CO_2, amounting to 1,122 kton per year for the AP shale gas and 569 kton per year for the GC shale gas.

Levelized Production Cost

Figure 12 demonstrates the financial variability in terms of the LCOPs. Overall, we can see that the LCOP depicts a wide distribution rather than squeezing around a single value. For example, the LCOP of the AP-H case study is subject to Weibull distribution. This indirectly indicates the insufficiency of deterministic analysis, which would provide a false impression of certainty in the outcomes of LCOP. In a vertical comparison, the histograms of LCOP distribution of the shale gas monetizing projects located in the same region but employing different production routes are presented. It is interesting that the case studies employing the NGLs pathway design has a much broader cost distribution. For example, as the monetization projects located in the AP region, the LCOP associated with the hybrid pathway ranges from $200/ton to $2,250/ton, while for the NGLs pathway design this value ranges from $-1,000/ton to $4,350/ton. This difference suggests that hybrid pathway design can effectively reduce the variability of production costs. It should be noted that a negative value of LCOP indicates that the monetizing project of interest is economically competitive even only considering the sale of by-products in some extreme scenarios.

In a horizontal comparison, the LCOP distributions of the monetizing project located at different shale regions but considering the same production route are investigated. As an example, when the hybrid pathway design is taken into account, the projects located in the AP region had a slightly narrower distribution of LCOP compared with the GC region case. In the case of the NGLs pathway design, the difference in the distribution width of LCOPs becomes wider and more apparent for the two shale regions investigated. This change can be mainly attributed to the variation of BEGPs shown in Figure 12. As shown, the production costs for

the GC region dominated by the variation of BEGP suffer a much greater variability (-$3.5/mmbtu ~48.2/mmbtu) compared with the AP region case ($2.5/mmbtu ~7.6/mmbtu).

(Place **Figure 12** here.)

To present the financial risk analysis, we consider that the LCOP cannot exceed a certain threshold, which is assumed to be $1,400/ton of HDPE according to the high level of market prices in the last three years.[74] Once the LCOP exceeds this value, the distributing range is marked by a translucent dashed-box and the resulting cumulative probability distributions (Ω_R) are provided in Figure 12. As shown in this figure, the monetizing projects considering the hybrid pathway design have a much lower financial risk in relation to the Ω_R. For example, the financial risk can be remarkably mitigated from 29.6% for the AP-O case study to 17.2% for the AP-H case study. This mitigation is mainly due to the following two facts (1) the former case study with a greater shale gas input (see Table 2) is much more vulnerable to the change in variable fuel cost; (2) an investment intensive OCM process involved in the hybrid pathway design requires larger fixed capital cost, which possesses less financial risk. Besides, under the same monetization option and operating conditions, the projects located in the GC region have a greater risk due to the greater variation in the BEGP of raw shale gas in this shale region (see Figure 13). However, note that this financial risk associated with the GC region case has a greater reduction in comparison with that associated with the AP region case, which is equal to 19.4% (from 37.80% to 18.5%).

(Place **Figure 13** here.)

Figure 14 compares the max-likelihood of LCOP results for different case studies with consideration of multi-refracturing treatments. Compared with the mean value shown in Figure 12, the MLE of LCOPs has a greater value by 8~12% for all case studies investigated. This increment clearly indicates that the true production cost is underestimated using the

conventional statistical method under uncertainty which, in turn, results in an over-optimistic forecast of financial risk. For each case study, first the refracturing treatment leads to a decrease in the MLE of LCOP, but when the number of well-refracturing continues to grow, the LCOP's MLE remarkably increases. The single refracturing treatment case (M=1) has the minimum MLE of LCOP, which is $975/ton for the AP-H case study, $1,038/ton for the AP-O case study, $994/ton for the GC-H case study, and $1,153/ton for the GC-O case study. This result suggests that a single refracturing treatment should be performed over the lifespan of the wells, which is sufficient to guarantee a minimum LCOP. Note that the optimal number of well-refractures comes from the EUR growth and nominal operation expense for an additional treatment. Furthermore, it can be forecasted that this number increases with the decline in the current well-restimulation cost of $ 0.8 MM.[10]

(Place **Figure 14** here.)

As has been concluded above, the hybrid pathway design provided an effective solution to reduce the financial risk of shale gas monetizing projects. The advantage is not limited to this aspect. For the GC region case shown in Figure 14, the hybrid pathway design can reduce the MLE of LCOPs by 10~15%, although this reduction significantly declines to about 5% for the AP region. This reflects that the hybrid pathway design is more amenable to reducing the risk of projects fed by raw shale gas that have high NGLs content. In other words, wet shale gas used as feedstock provides an opportunity to perform the process integration and equipment sharing considered in the hybrid pathway design, as NGLs are comparable to the methane in terms of the feed amount; otherwise, the improvement on the real production cost is not as much as anticipated.

Plant-level GHG Emissions

In Figure 15, we present the GWP distributions for the unit HDPE production according to the gate-to-gate LCA analysis. All the LCOP distributions are narrow and symmetric, which approximately follows the normal distribution, indicating the linear relationship between the inputs and outputs. As illustrated in Figure 6(E), only the hybrid pathway design employs a proactive CCS operation to mitigate the GHG emissions through recovering around 98% of process CO_2 from the OCM reactor effluent. As a result, Figure 15 illustrates that the GWP distribution associated with the hybrid pathway design is reduced to 0.88-1.08 kg CO_2-eq/kg HDPE for the AP shale gas, and 0.85-1.06 kg CO_2-eq/kg HDPE for the GC shale gas. In a vertical comparison, the hybrid pathway design exhibits a lower level of GWP distribution, which is lower than that of the NGLs pathway design, byabout 30% on average. Meanwhile, given the same monetization pathway, we can observe that the GWP distribution of the AP region case is higher than that of the GC region case by only 4–6%. The major reason for this slight increase in GWP related to the feedstock composition will be discussed as follows.

(Place **Figure 15** here.)

(Place **Figure 16** here.)

Figure 16 shows the breakdown of MLE of GWPs for different process designs. Note that the influences of gas/NGL pipelines on carbon footprints are not taken into account due to their ignorable impacts. In this figure, when the multi-refracturing treatment is not employed (M=0), the MLEs of GWPs for the AP-H, AP-O, GC-H, and GC-O case studies amount to 1.01, 1.43, 0.95, and 1.34 kg CO_2-eq/kg HDPE, respectively, which is exactly equal to the mean values of GWPs provided in Figure 15. For each case study, the centralized polymers production has a similar MLE (about 0.82 kg CO_2-eq/kg HDPE), which contributes the largest share (82–86%) of the total GHG emissions. The distributed shale gas processing facility is a minor contributor to the GWP, but this contribution obviously varies from design to design. This phenomenon is

because, on one hand, the high NGLs content for the GC shale gas helps to decrease its required number of wet wells and shale gas processing facilities, thus reducing the absolute GHG emissions during the gas processing. On the other hand, NGL content is related to the calculation of allocating factor. As listed in Table 1, all the case studies have the same capacities for polymers production. However, the GC-O and GC-H case studies generate much smaller amounts of low price PG, indirectly increasing the allocation factor based on economic value in relation to the HDPE. Besides, for each case study, the multi-refracturing treatment has a slight impact on the MLE of GWPs, because a higher EUR can only decrease the total GHG emissions in relation to the gas processing by decreasing the required number of processing facilities.

Conclusions

This article developed a systematic monetization framework that incorporates stochastic modeling and likelihood analysis of a large-scale shale gas monetization process. The major products investigated in this work were polymers including HDPE and PP. The mixed uncertainty considered in the monetization framework not only included endogenous variabilities of gas composition and EUR, but also the exogenous ones of the entire project, often corresponding to market variabilities. To accommodate the reality of uncertainty, a new stochastic data processing strategy integrating the SAA, KSM, and DSAC methods was proposed to generate appropriate scenarios and to determine the corresponding values of each uncertain variable. These output variabilities were passed to the process simulator to implement the detailed process design and techno-economic analysis. A distributed-centralized conversion network employing two monetization pathways of shale gas to polymers, namely NGLs pathway and hybrid pathway, was presented. Uncertain economic parameters were nested in

this stochastic model to identify the probabilistic distributions and to analyze the MLE of techno-economic-environmental objectives.

The proposed framework was applied to four case studies based on different plant locations (AP and GC shale regions) and the above mentioned pathways. The results highlighted the benefits of the hybrid pathway as it reduced the MLE of LCOPs and had a much greater potential in GHG mitigation. In particular, the hybrid pathway design is more amenable to reducing the economic risk of the projects located in the GC shale region where the raw shale gas has appropriate NGLs content but suffers from expensive extraction expenses.

Acknowledgment

Financial supports from the National Natural Science Foundation of China (No. 21606261 and No. U1462113) are gratefully acknowledge.

Notation

Sets and indices

GHGs: greenhouse gases indexed by g

$\boldsymbol{I}$: set of sampled wells indexed by i

$\boldsymbol{J}$: set of components indexed by j

$\boldsymbol{P}$: set of initial gas production rate indexed by P

r: set of correlation of sample points and new-added points

x: input data set used in Kriging interpolation

s: index for scenario

y: output data set generated by Kriging interpolation

Greek Symbols

β: peak reduction ratio

γ: initial fracture contribution

δ: confidence interval

η: economic value-based allocating factor

θ: adjustable parameter

λ: amount of equivalent CO_2 emissions

μ: empirical coefficient

v: empirical coefficient

π: terrain factor

σ^2: process covariance

φ: damage factor

ϕ: decline steepness increase

Ψ: new-added points

ω: sample points

Ω_R: cumulative probability

Parameters and variables

AF: annual feedstock cost

AO: annual operating cost

AP: annual production

AT: annual operating time

b: decline exponent

bp: by-product

$CO_{2\text{-}eq}$: equivalent CO_2 emissions

CR: consumption rate

$C_{i,j}$: concentration of component *j* from well *i*

DR: discount rate

drt: refracture treatment duration

$\overline{d_c}$: average distance from the processing facility to production plant

$\overline{d_p}$: average distance from the well-site to processing facility

D_i: initial decline rate

f: the ratio of wet wells to total wells

g: discharge

M: mean value

MF: mass flow rate

MW_{SEG}: average segment molecular weight

$\overline{MSE}$: mean value of MSE

m: refracturing treatment times

n: sample size

*N**: initial scenarios generated by SAA method

$N^{\dagger}$: scenarios corresponds to the wet wells

N^{+}: sub-scenarios specified in the Monte Carlo simulation

N^{Θ}: sub-scenarios used in the likelihood analysis

$P_i^{t_0}$: initial gas production rate of well *i*

$P_{i,j}^{t_0}$: initial production rate of component *j* of well *i*

$\overline{P_{i,C_1}^{t_0}}$: expected initial value of methane production rate of sampled wells

$P_{s,C_1}^{t_0}$: initial methane production rate corresponds to scenario *s*

P_s^t : production rate corresponds to scenario *s*

q_c: capacity of the polymers production plant

q_P: capacity of the processing facility

R: revenue

RV: residual value

S: specification

T_{ls}: lifespan

TPC: total plant capital cost

trt: the timing of the refracture treatment

t_0: extraction beginning date

u: utility

var: variance estimator

WF: weight fraction

Δt_i: interval between the refractures

Y_{rg}: raw gas extraction per square mile

Y_{wg}: wet gas extraction per square mile

z: noisy information

$z_{\alpha/2}$: standard normal deviation

Units

bscf: billion square cubic feet

mmscfd: million square cubic feet per day

Mt: million metric tons

Nomenclature

AGE: acid gas enrichment

AGR: acid gas removal

AP: Appalachian

ASU: air separation unit

BEGP: breakeven gas price

CP: centralized polymers production plant

CW: cooling water

DACE: design and analysis of computer experiments

DFs: distributed shale gas processing facilities

DSAC: decline-stimulate analysis curve

E-P: ethane-propane

EUR: estimated ultimate recovery

FCPW: full-cycle per-well

FBR: fluidized-bed reactor

F-T: Fischer-tropsch

GC: Gulf Coast

GWP: global warming potential

H: polymers are derived from hybrid NGLs and methane

HDPE: high-density polyethylene

HHV/hhv: high heating value

HPF: high pressure flasher

IQR: interquartile range

KSM: Kriging-based surrogate model

LHV: low heating value

LPF: low pressure flasher

LCOP: levelized production cost of polymers

LP: low pressure

LPG: liquid petroleum gas

MD: median

MDEA: methyl-diethanolamine

MED: multi-effect distillation

MLE: max-likelihood estimation

MP: middle pressure

MSE: mean-squared error

N: normal distribution

NGLs: natural gas liquids

O: polymers are derived from NGLs only

OCM: coupling of methane

P: probability

PDI: poly-dispersity index

PE: poly-ethylene

PG: pipeline gas

PP: poly-propene

PSA: pressure swing adsorption

R**:** spatial correlation function

RT: refracturing treatment

SAA: sample average approximation

SCOT: Shell Claus Off-gas Treating

S_i: the i^{th} step

SP: stochastic programming

TEG: triethylene glycol

TDS: total dissolved solids

TO: tight oil

U: uniform distribution

WWT: wastewater treatment

Literature cited

1. EIA. Natural Gas Futures Prices (NYMEX). In: EIA, ed. Washington, DC: Henry Hub; 2016.
2. Gao J, You F. Design and optimization of shale gas energy systems: Overview, research challenges, and future directions. Computers & Chemical Engineering. 2017; 106(2):699-718.
3. Statista. Global plastic production from 1950 to 2014 (in million metric tons). 2014; https://www.statista.com/. Accessed 21/05, 2017.
4. Keller GE, Bhasin M. Synthesis of ethylene via oxidative coupling of methane: I. Determination of active catalysts. Journal of Catalysis. 1982;73(1):9-19.
5. He C, You F. Towards More Cost-Effective and Greener Chemicals Production from Shale Gas by Integrating with Bioethanol Dehydration: Novel Process Design and simulation-based Optimization. AIChE Journal. 2014;61(4):1209-1232.
6. Liu P, Georgiadis MC, Pistikopoulos EN. Advances in Energy Systems Engineering. Ind Eng Chem Res. 2011;50(9):4915-4926.
7. Gong J, You F. Sustainable design and synthesis of energy systems. Current Opinion in Chemical Engineering. 2015;10:77-86.
8. Li X, Armagan E, Tomasgard A, Barton PI. Stochastic pooling problem for natural gas production network design and operation under uncertainty. AIChE Journal. 2011;57(8):2120-2135.
9. Gong J, Yang M, You F. A systematic simulation-based process intensification method for shale gas processing and NGLs recovery process systems under uncertain feedstock compositions. Computers & Chemical Engineering. 2016; 105 (4):259-275.
10. Cafaro DC, Drouven MG, Grossmann IE. Optimization models for planning shale gas well refracture treatments. AIChE Journal. 2016;62(12):4297-4307.

11. Drouven MG, Cafaro DC, Grossmann IE. Stochastic Programming Models for Optimal Shale Well Development and Refracturing Planning under Uncertainty. AIChE Journal. 2017; 63(11):4799-4813.
12. Tavassoli S, Yu W, Javadpour F, Sepehrnoori K. Well Screen and Optimal Time of Refracturing: A Barnett Shale Well. Journal of Petroleum Engineering. 2013;2013:1-10.
13. Grossmann IE, Apap RM, Calfa BA, Garcia-Herreros P, Zhang Q. Recent Advances in Mathematical Programming Techniques for the Optimization of Process Systems under Uncertainty. In: Krist V. Gernaey JKH, Rafiqul G, eds. Computer Aided Chemical Engineering. Vol 37: Elsevier; 2015:1-14.
14. Gao J, He C, You F. Shale Gas Process and Supply Chain Optimization: Springer International Publishing; 2017.
15. Siirola JJ. The Impact of Shale Gas in the Chemical Industry. Aiche Journal. 2014;60(3):810-819.
16. Onel O, Niziolek AM, Floudas CA. Integrated biomass and fossil fuel systems towards the production of fuels and chemicals: state of the art approaches and future challenges. Current Opinion in Chemical Engineering. 2015;9:66-74.
17. Ehlinger VM, Gabriel KJ, Noureldin MMB, El-Halwagi MM. Process Design and Integration of Shale Gas to Methanol. ACS Sustainable Chemistry & Engineering. 2013;2(1):30-37.
18. Julián-Durán LM, Ortiz-Espinoza AP, El-Halwagi MM, Jiménez-Gutiérrez A. Techno-Economic Assessment and Environmental Impact of Shale Gas Alternatives to Methanol. Acs Sustainable Chemistry & Engineering. 2014;2(10):2338-2344.

19. Niziolek AM, Onel O, Floudas CA. Production of benzene, toluene, and xylenes from natural gas via methanol: Process synthesis and global optimization. AIChE Journal. 2015;62(5):1531-1556.

20. Niziolek AM, Onel O, Elia JA, Baliban RC, Floudas CA. Coproduction of liquid transportation fuels and C6_C8 aromatics from biomass and natural gas. AIChE Journal. 2015;61(3):831-856.

21. Derosa SE, Allen DT. Impact of New Manufacturing Technologies on the Petrochemical Industry in the United States: A Methane-to-Aromatics Case Study. Industrial & Engineering Chemistry Research. 2016;55(18):5366-5372.

22. Onel O, Niziolek AM, Floudas CA. Optimal Production of Light Olefins from Natural Gas via the Methanol Intermediate. Industrial & Engineering Chemistry Research. 2016;55(11):3043–3063.

23. Baliban R, Elia J, Floudas C. Novel Natural Gas to Liquids Processes: Process Synthesis and Global Optimization Strategies. Aiche Journal. 2013;59(2):505-531.

24. Guo X, Fang G, Li G, et al. Direct, Nonoxidative Conversion of Methane to Ethylene, Aromatics, and Hydrogen. Science. 2014;344(6184):616-619.

25. Siluria I. Siluria & Braskem to explore deployment of Siluria's OCM technology for making ethylene from natural gas. Focus on Catalysts. 2014;2014:6–7.

26. Salkuyeh YK, Ii TAA. A novel polygeneration process to co-produce ethylene and electricity from shale gas with zero CO 2 emissions via methane oxidative coupling. Energy Conversion & Management. 2015;92(92):406-420.

27. Yao Y, Graziano DJ, Riddle M, Cresko J, Masanet E. Understanding Variability To Reduce the Energy and GHG Footprints of U.S. Ethylene Production. Environmental Science & Technology. 2015;49(24):14704-14716.

28. Yang M, You F. Comparative Techno-Economic and Environmental Analysis of Ethylene and Propylene Manufacturing from Wet Shale Gas and Naphtha. Industrial & Engineering Chemistry Research. 2017;56(14):4038-4051.

29. He C, You F. Shale Gas Processing Integrated with Ethylene Production: Novel Process Designs, Exergy Analysis, and Techno-Economic Analysis. Industrial & Engineering Chemistry Research. 2014;53(28):11442-11459.

30. He C, You F. Deciphering the true life cycle environmental impacts and costs of the mega-scale shale gas-to-olefins projects in the United States. Energy Environ Sci. 2016;9(3):820-840.

31. Baliban RC, Elia JA, Floudas CA. Biomass and Natural Gas to Liquid Transportation Fuels: Process Synthesis, Global Optimization, and Topology Analysis. Industrial & Engineering Chemistry Research. 2013;52(9):3381-3406.

32. Martín M, Grossmann IE. Optimal use of hybrid feedstock, switchgrass and shale gas for the simultaneous production of hydrogen and liquid fuels. Energy. 2013; 55(1):378-391.

33. Salkuyeh YK, Thomas II. Co-Production of Olefins, Fuels, and Electricity from Conventional Pipeline Gas and Shale Gas with Near-Zero CO2 Emissions. Part II: Economic Performance. Energies. 2015;8(5):3762-3774.

34. Wang MQ, Xu Q. Optimal design and operation for simultaneous shale gas NGL recovery and LNG re-gasification under uncertainties. Chem Eng Sci. 2014;112:130-142.

35. Diwekar UM, Rubin ES. Stochastic modeling of chemical processes. Computers & Chemical Engineering. 1991;15(2):105-114.

36. Salazar JM, Diwekar UM, Zitney SE. Stochastic Simulation of Pulverized Coal (PC) Processes. Energy Fuels. 2010;24(9):4961-4970.

37. Ren T, Patel M, Blok K. Steam cracking and methane to olefins: Energy use, CO2 emissions and production costs. Energy. 2008;33(5):817-833.

38. Gao J, You F. Deciphering and handling uncertainty in shale gas supply chain design and optimization Novel modeling framework and computationally efficient solution algorithm. AIChE Journal. 2015;61(11):3739-3755.

39. Gebreslassie BH, Yao Y, You F. Design under uncertainty of hydrocarbon biorefinery supply chains Multiobjective stochastic programming models, decomposition algorithm, and a Comparison between CVaR and downside risk. AIChE Journal. 2012; 58(7):2155-2179.

40. EIA. Hydrocarbon Gas Liquids (HGL): Recent Market Trends and Issues. Washington, DC: U.S. Energy Information Administration;2014.

41. Baihly JD, Altman RM, Malpani R, Luo F. Shale gas production decline trend comparison over time and basins. Paper presented at: SPE annual technical conference and exhibition, 2010.

42. Caballero JA, Grossmann IE. An algorithm for the use of surrogate models in modular flowsheet optimization. AIChE Journal. 2008;54(10):2633-2650.

43. Davis E, Ierapetritou M. A kriging method for the solution of nonlinear programs with black-box functions. AIChE Journal. 2007;53(8):2001-2012.

44. Cozad A, Sahinidis NV, Miller DC. Learning surrogate models for simulation-based optimization. AIChE Journal. 2014;60(6):2211-2227.

45. Lophaven SN, Nielsen HB, Søndergaard J. A MATLAB Kriging Toolbox: Version 2.0. Lyngby, Denmark 2002.

46. Quirante N, Javaloyes J, Caballero JA. Rigorous design of distillation columns using surrogate models based on Kriging interpolation. AIChE Journal. 2015;61(7):2169-2187.

47. Zavalaaraiza D, Allen DT, Harrison M, George FC, Jersey GR. Allocating Methane Emissions to Natural Gas and Oil Production from Shale Formations. ACS Sustainable Chemistry & Engineering. 2015;3(3):492-498.

48. Mokhatab S, Poe WA. Chapter 7 - Natural Gas Sweetening. In: Mokhatab S, Poe WA, eds. Handbook of Natural Gas Transmission and Processing (Second Edition). Boston: Gulf Professional Publishing; 2012:253-290.

49. He C, You F. Deciphering the true life cycle environmental impacts and costs of the mega-scale shale gas-to-olefins projects in the United States. Energy Environ Sci. 2016; 9:820-840.

50. Parks LE, Perry D, Fedich R. FLEXSORB ®SE A Proven Reliable Acid Gas Enrichment Solvent. In: Benyahia F, Eljack FT, eds. Proceedings of the 2nd Annual Gas Processing Symposium. Vol 2. Amsterdam: Elsevier; 2010:229-235.

51. Mokhatab S, Poe WA. Chapter 8 - Sulfur Recovery and Handling. In: Mokhatab S, Poe WA, eds. Handbook of Natural Gas Transmission and Processing (Second Edition). Boston: Gulf Professional Publishing; 2012:291-316.

52. He C, You F. Shale Gas Processing Integrated with Ethylene Production: Novel Process Designs, Exergy Analysis, and Techno-Economic Analysis. Industrial & Engineering Chemistry Research. 2014;53(28):11442-11459.

53. Z. Stansch, L. Mleczko A, Baerns M. Comprehensive Kinetics of Oxidative Coupling of Methane over the La2O3/CaO Catalyst. Industrial & Engineering Chemistry Research. 1997;36(7):2568-2579.

54. Field RP, Brasington R. Baseline Flowsheet Model for IGCC with Carbon Capture. Ind. Eng. Chem. Res. 2011;50(19):11306-11312.

55. Chin SY, Radzi SNR, Maharon IH, Shafawi MA. Kinetic model and Simulation Analysis for Propane Dehydrogenation in an Industrial Moving Bed Reactor. World Academy of Science Engineering & Technology. 2011; 52:165-183.

56. Froment GP, Van de Steene BO, Van Damme PS, Narayanan S, Goossens AG. Thermal Cracking of Ethane and Ethane-Propane Mixtures. Industrial & Engineering Chemistry Process Design and Development. 1976;15(4):495-504.

57. Froment GF, Van De Steene BO, Vanden Berghe PJ, Goossens AG. Thermal cracking of light hydrocarbons and their mixtures. AIChE Journal. 1977;23(1):93-106.

58. Loc LC, Gaidai NA, Kiperman SL, Thoang HS. Kinetics of Propane and n-Butane Dehydrogenation over Platinum-Alumina Catalysts in the Presence of Hydrogen and Water Vapor. Kinetics & Catalysis. 1996;37(6):790-796.

59. Herzog HJ. Peer Reviewed: What Future for Carbon Capture and Sequestration? Environmental Science & Technology. 2001;35(7).

60. Anderson S, Newell R. Prospects for Carbon Capture and Storage Technologies. General Information. 2003;29(2):109-142.

61. Bhattacharyya D, Turton R, Zitney SE. Steady-State Simulation and Optimization of an Integrated Gasification Combined Cycle Power Plant with CO2 Capture. Industrial & Engineering Chemistry Research. 2010;50(3):1674-1690.

62. Aspentech. Aspen Polymers: Examples & Applications. Burlington, MA: Aspen Technology, Inc.; 2010.

63. Kissin YV. Isospecific polymerization of olefins with heterogeneous Ziegler-Natta catalysts: Springer-Verlag; 1985.

64. Gabriel KJ, Linke P, Jiménez-Gutiérrez A, Martínez DY, Noureldin M, El-Halwagi MM. Targeting of the water-energy nexus in gas-to-liquid processes: A comparison of

syngas technologies. Industrial & Engineering Chemistry Research. 2014;53(17):7087-7102.

65. Martínez DY, Jiménez-Gutiérrez A, Linke P, Gabriel KJ, Noureldin MMB, El-Halwagi MM. Water and Energy Issues in Gas-to-Liquid Processes: Assessment and Integration of Different Gas-Reforming Alternatives. ACS Sustainable Chemistry & Engineering. 2014;2(2):216-225.

66. Berman A. After the gold rush: A perspective on future US natural gas supply and price. Energy Bulletin. 2012.

67. Initiative ME. The Future of Natural Gas: Appendix 2D Shale Gas Economic Sensitivities: Cambridge, MA; 2011.

68. GREET. The greenhouse gases, regulated emissions, and energy use in transportation model. Oak Ridge, TN: Argonne National Laboratory; 2012.

69. A Competence Centre of ETH, PSI, Empa and ART. ecoinvent data Swiss Centre for Life Cycle Inventories; 2009. Accessed 21/05, 2017.

70. Allen DT, Torres VM, Thomas J, et al. Measurements of methane emissions at natural gas production sites in the United States. Proceedings of the National Academy of Sciences of the United States of America. 2013;110(44):17768.

71. Genest C, Remillard B, Beaudoin D. Goodness-of-fit tests for copulas: A review and a power study. Insurance Mathematics & Economics. 2009;44(2):199-213.

72. EIA. Review of Emerging Resources: U.S. Shale Gas and Shale Oil Plays. EnergyWashington, DC: U.S. Energy Information Administration;2011.

73. Hughes JD. Drilling Deeper: A reality check on US government forecasts for a lasting tight oil and shale gas boom. Post Carbon Institute, California. 2014.

74. http://www.plastemart.com/polymer-price-list-pe-pp-pvc, Accessed 21/05, 2017.

Appendix

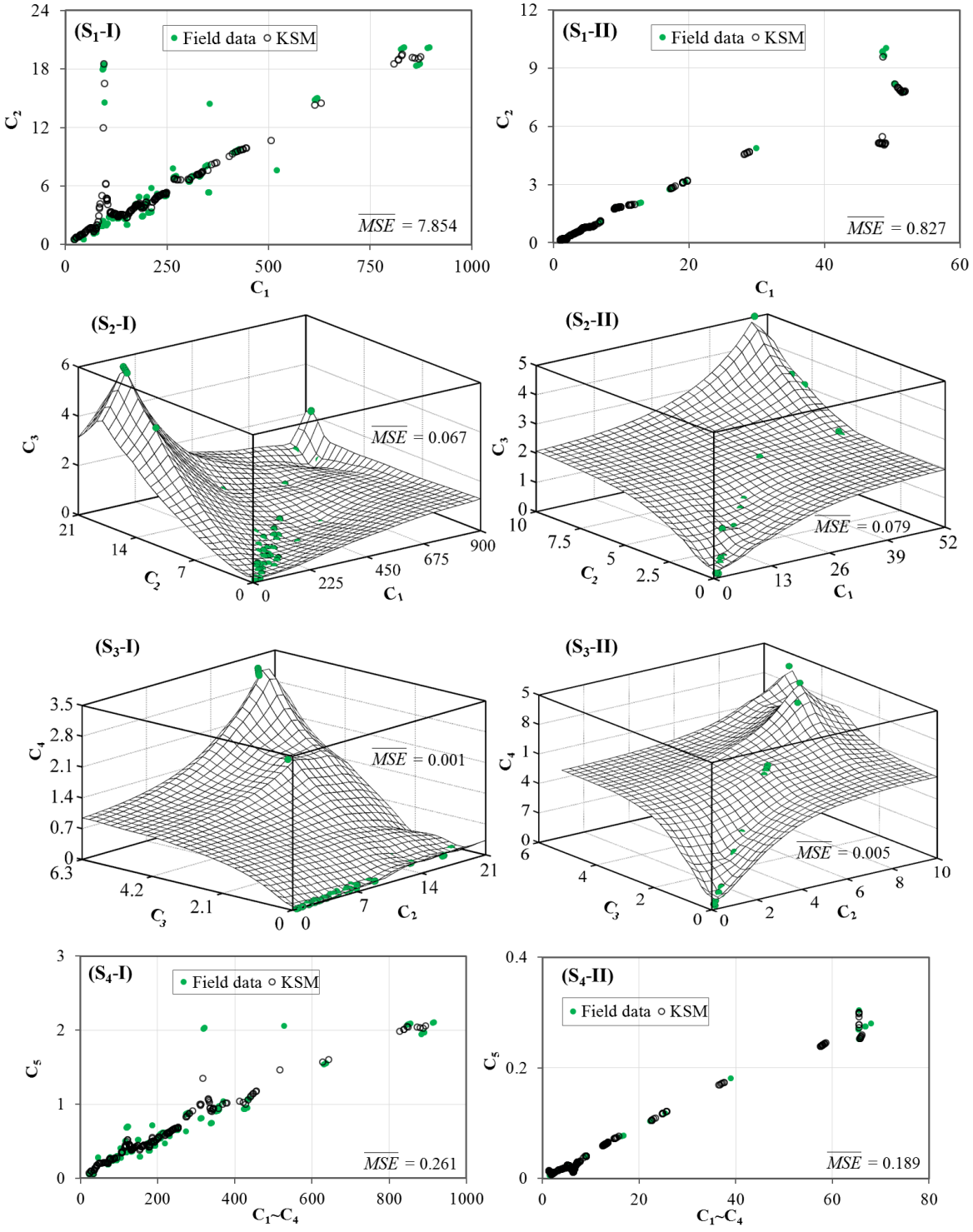
(S1-I)
Field data KSM
$\overline{MSE}$ = 7.854
C2
C1
(S1-II)
Field data KSM
$\overline{MSE}$ = 0.827
C2
C1
(S2-I)
$\overline{MSE}$ = 0.067
C3
C2
C1
(S2-II)
$\overline{MSE}$ = 0.079
C3
C2
C1
(S3-I)
$\overline{MSE}$ = 0.001
C4
C3
C2
(S3-II)
$\overline{MSE}$ = 0.005
C4
C3
C2
(S4-I)
Field data KSM
$\overline{MSE}$ = 0.261
C5
C1~C4
(S4-II)
Field data KSM
$\overline{MSE}$ = 0.189
C5
C1~C4

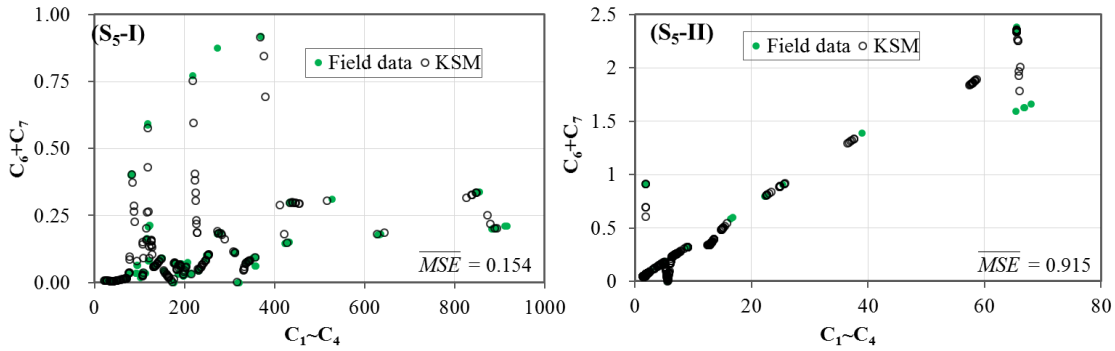

Figure A-1. Comparisons of field data and predicted results by the KSM. (I) AP shale region and (II) RM shale region.

List of Table Captions

Table 1. Model Parameter Specifications

Parameter	Specification	Units	Note
SAA			
confidence interval, δ_d	0.95	[-]	[38]
DSAC			
decline exponent [a], b	AP:1.5090 GC:1.2065	[-]	[10,12]
initial decline rate [a], D_i	AP:0.2540 GC:0.2522	[-]	[10,12]
extraction beginning date, t_0	2	[mon]	[10,12]
refracture treatment duration, drt	1	[mon]	[10,12]
interval between the refractures, Δt_i	35	[mon]	[10,12]
decline steepness increase, ϕ	1.5×10^{-3}	[1/mon]	[10,12]
well lifespan, T_{ls}	20	[y]	[30]
peak reduction ratio, β_i	0.4/0.36/0.32	[-]	[10,12]
initial fracture contribution, γ	1	[-]	[10,12]
Feedstock transportation			
well spacing	AP:0.13 GC:0.15	[wells/sq. mile]	[72,73]
terrain factor, π	1.2	[-]	[27,28]
Likelihood estimation			
electricity	U(0.04, 0.1)[b]	[$/kwh]	[9,49]
refrigerant	U(7, 10)	[$/mmbtu]	[49]
cooling/boiling water	U(0.01, 0.06)	[$/ton]	[49]
solvent (DEA, MDEA, TEG)	U(2000, 3400)	[$/ton]	[28,49]
LP heat	U(8.5, 12.5)	[$/GJ]	[49]
MP heat	U(10, 14)	[$/GJ]	[49]
drilling investment	U(0.6, 1.0)	[$MM]	[10]
PG	U(2.7, 3.7)	[$/mmbtu]	[1]
butanes+	U(0.5, 0.9)	[$/gal]	[9]
PP	U(1,150, 1,350)	[$/ton]	[74]
sulfur	U(100, 300)	[$/ton]	[49]
hydrogen	U(1.3, 2.2)	[$/kg]	[29]

[a] The decline exponent and initial decline rate are regressed from the field data listed in Tables S-13 and S-14 in SI.

[b] U denotes a uniform distribution.

Table 2. Summary of Process-level Techno-economic Results

	AP-H	AP-O	GC-H	GC-O
Transportation*				
Processing facility, n	6	23	2	3
Wet wells, n	291	1,167	605	1,016
$\overline{d_p}$, mile	1.0	1.0	1.6	1.6
$\overline{d_c}$, mile	1.8	1.8	2.5	2.5
Feedstock				
Shale gas, mmscfd	321	1,175	203	342
NGLs				
NGLs, ton/h	11.1	43.1	37.3	62.5
Utilities				
Net power, MW	-85.8	23.7	12.5	46.8
Net water, ton/h	158	187	142	172
LP heat, MW	861	265	32.1	27.4
MP heat, MW	486	679	806	388
Cold energy, MW	577	428	583	443
Solvents, kg/h	40.8	98.2	53.4	112.5
Process yield				
HDPE, kton/y	284	268	232	193
PP, kton/y	9.6	26.0	62.1	101
PG, mmscfd	149	1,065	94.7	293
Butanes+, bbl/y	7,594	36,184	4,347	7,268
Sulfur, kton/y	1.5	5.9	9.75	17.6
TO, mmbbl/y	0	0	4.5	7.5
GHG emissions				
CO_2 captured, kton/y	1,122	0	569	0
CO_2 emission, kton/y	1,050	508	595	984
Capital cost[a]				
DFs, MM$	108	443	95.4	144
CP, MM$	576	220	447	178

[a] The following investments are not taken into account (1) equipment used in olefins polymerization unit including extrusion die, pelletizer, centrifugal dewater, package machine, etc.; (2) land acquisition and use, building construction, worker training, etc.